

Interferometric synthetic aperture radar (InSAR) atmospheric correction: GPS, Moderate Resolution Imaging Spectroradiometer (MODIS), and InSAR integration

Zhenhong Li, Jan-Peter Muller, and Paul Cross

Department of Geomatic Engineering, University College London, London, UK

Eric J. Fielding

Jet Propulsion Laboratory, California Institute of Technology, Pasadena, California, USA

Department of Earth Sciences and Bullard Laboratories, University of Cambridge, Cambridge, UK

Received 20 September 2004; revised 28 December 2004; accepted 14 January 2005; published 31 March 2005.

[1] Atmospheric effects represent one of the major limitations of repeat-pass interferometric synthetic aperture radar (InSAR). In this paper, GPS, and Moderate Resolution Imaging Spectroradiometer (MODIS) data were integrated to provide regional water vapor fields with a spatial resolution of $1 \text{ km} \times 1 \text{ km}$, and a water vapor correction model based on the resultant water vapor fields was successfully incorporated into the Jet Propulsion Laboratory/California Institute of Technology ROI_PAC software. The advantage of this integration approach is that only one continuous GPS station is required within a $2030 \text{ km} \times 1354 \text{ km}$ MODIS scene. Application to ERS-2 repeat-pass data over the Los Angeles Southern California Integrated GPS Network (SCIGN) area shows that this integration approach not only helps discriminate geophysical signals from atmospheric artifacts but also reduces water vapor effects significantly, which is of great interest to a wide community of geophysicists.

Citation: Li, Z., J.-P. Muller, P. Cross, and E. J. Fielding (2005), Interferometric synthetic aperture radar (InSAR) atmospheric correction: GPS, Moderate Resolution Imaging Spectroradiometer (MODIS), and InSAR integration, *J. Geophys. Res.*, *110*, B03410, doi:10.1029/2004JB003446.

1. Introduction

[2] The propagation delay of radio signals through the neutral atmosphere is a dominant source of error in repeat-pass Interferometric SAR (InSAR). *Massonnet et al.* [1994] first identified atmospheric effects in repeat-pass InSAR measurements when they studied the 1992 Landers earthquake. *Goldstein* [1995] found that the interferogram acquired over the Mojave Desert in California by the Shuttle Imaging Radar satellite (SIR-C) contained one-way path delays with a peak value of 2.8 cm and a root-mean-square (RMS) error of ~ 0.3 cm. *Rosen et al.* [1996] reported that two-way path delays due to atmospheric refractivity anomalies were found at the level of a 12 cm peak-to-peak amplitude in the line of sight (LOS) direction over Kilauea Volcano, Hawaii. *Zebker et al.* [1997] suggested that a 20% spatial or temporal change in relative humidity could result in a 10–14 cm error in deformation measurement retrievals, independent of baseline parameters, and possibly 80–290 m of error in derived digital elevation models (DEM) for those interferometric pairs with unfavorable baseline geometries. Several techniques have been proposed for reducing atmospheric effects in

interferograms, including stacking and calibration. Stacking involves temporal averaging of N -independent interferograms to reduce the temporally uncorrelated noise by $1/\sqrt{N}$ [*Zebker et al.*, 1997], while calibration involves spatial reduction (if not complete removal) of path delays using independent data such as continuous Global Positioning System (GPS) networks [*Bock and Williams*, 1997; *Williams et al.*, 1998]. A disadvantage of the use of GPS data to correct InSAR measurements is that a dense GPS network is required which is usually not available, especially in remote areas.

[3] Space-based monitoring is an effective way to obtain a measurement of the water vapor distribution on a global basis with a spatial resolution much closer to SAR images than the station spacing of GPS networks. The NASA Moderate Resolution Imaging Spectroradiometer (MODIS) is a key instrument on the Terra and Aqua satellites, launched on 18 December 1999 and 4 May 2002, respectively. The Terra platform flies in a near-polar, Sun-synchronous orbit, as does the ERS-2 satellite that carries the Active Microwave Instrument (AMI) Synthetic Aperture Radar (SAR). Both have a descending node across the equator at around 10:30 am local time. The MODIS instrument images a wide swath of around 2330 km across [*Nishihama et al.*, 1997]. This enables MODIS water vapor data to be used to correct daytime ERS-2 InSAR measure-

ments. We found that there was a MODIS image acquired within an hour of each of the ERS scenes used here. In this study, we integrate GPS and MODIS data to provide high spatial resolution water vapor fields to correct InSAR measurements.

[4] A short description of MODIS and GPS data is given in section 2, followed by a GPS/MODIS integrated model developed to produce high spatial resolution two-dimensional (2-D) water vapor fields in section 3. The test area is described followed by a brief introduction to a water vapor correction approach designed and implemented in this study in section 4. In section 5, the application of the GPS/MODIS integrated correction model to the Southern California Integrated GPS Network (SCIGN) is demonstrated. Finally, conclusions and a short outlook on future work are presented in section 6.

2. Water Vapor Product Descriptions

2.1. MODIS Near-IR Water Vapor Product

[5] The MODIS instrument is a passive imaging spectroradiometer providing high radiometric sensitivity (12 bit) in 36 spectral bands ranging in wavelength from 0.4 μm to 14.4 μm . Two bands are imaged at a nominal resolution of 250 m at nadir, with five bands at 500 m and the remaining 29 bands at 1,000 m. A $\pm 55^\circ$ scanning pattern at the Terra (or Aqua) orbit of 705 km achieves a 2330-km swath and provides global coverage every 1 to 2 days [Nishihama *et al.*, 1997].

[6] Five near-infrared (IR) MODIS channels are useful for remote sensing of water vapor with three water vapor absorption and two nonabsorption channels [Gao and Kaufman, 2003]. The technique implemented for MODIS water vapor retrievals relies on observations of water vapor attenuation of reflected solar radiation in the near-IR channels. As a result, the MODIS near-IR precipitable water vapor amount (designated hereafter as MODIS-PWV) can only be measured during the daytime and stored in the MOD05 product. This product includes a cloud mask, geolocation data, and scan time. The current resolution of MODIS-PWV is 1×1 km (at nadir), and the output grid of a single level 2 MODIS water vapor product is 2030 1-km pixels in width (across the swath) and 1354 1-km pixels in length (along the swath).

[7] MODIS-PWV is claimed to be determined with an accuracy of 5–10%, and errors will be greater for retrievals from data collected over dark surfaces or under hazy conditions [Gao and Kaufman, 2003]. Extensive comparisons among radiosondes, GPS and MODIS water vapor products showed that MODIS-PWV (collection 3) appeared to overestimate water vapor compared to GPS and radiosonde values with scale factors ranging from 1.07 to 1.20; indicating that MODIS-PWV should be calibrated (e.g., using a linear model) before being applied to correct InSAR atmospheric effects [Li *et al.*, 2003]. A scale factor of 1.05 was observed previously [Li, 2004] for the Terra MODIS-PWV collection 4 products that were used in this study. It should be noted that there is no change in the water vapor retrieval algorithm, but an update of calibration lookup tables for the MODIS level 1B (L1B) radiances between MODIS-PWV collections 3 and 4 (B.-C. Gao, private communication, 2003).

[8] For the purpose of InSAR atmospheric correction, MODIS-PWV needs to be converted into zenith wet delay (ZWD) using the following relationship:

$$\text{ZWD} = \text{PWV}/\Pi \quad (1)$$

where Π is a dimensionless conversion factor, approximately equal to 6.2. This factor is dependent on the weighted mean temperature of the atmosphere and can be inferred either from surface temperature measurements or from numerical weather models with an accuracy of about 2% or better [Bevis *et al.*, 1992]. The mean temperature of the atmosphere (T_m) used in this study was determined by [Bevis *et al.*, 1992]:

$$T_m = 70.2 + 0.72T_S \quad (2)$$

where T_S is the surface temperature, in kelvins, and was obtained from GPS meteorological data in this study. In this study, equations (1) and (2) were also used to convert GPS ZWD estimates into PWV.

2.2. GPS

[9] In this paper, if not specified, the GPS data were analyzed separately for each UTC day using the GIPSY-OASIS II software package in precise point positioning mode [Zumberge *et al.*, 1997]. Phase measurements were decimated to 300 s in the analysis. The receiver's clock was modeled as a white noise process with updates at each measurement epoch, and ZWD was modeled as a random walk with a sigma of 10.2 mm/ $\sqrt{\text{h}}$. The gradient parameters, G_N and G_E , were modeled as random walk processes with a sigma of 0.3 mm/ $\sqrt{\text{h}}$. Satellite final orbits and clocks were obtained via anonymous FTP (<ftp://sidshow.jpl.nasa.gov/pub>) from the Jet Propulsion Laboratory (JPL).

[10] As demonstrated by Li *et al.* [2003], tropospheric delay was estimated in two steps: First, the tropospheric delay was determined together with the site position and receiver clock. Then the site position was fixed to the average of that day, and only the zenith tropospheric delays and receiver clocks were estimated. This was done because of the high correlation between height and the part of zenith tropospheric delay (ZWD) due to water vapor. In other words, real variations in ZWD may manifest themselves as apparent variations in height. Therefore retrievals of ZWD will be obtained with less reliability if the height and ZWD need to be estimated simultaneously.

[11] In order to separate ZWD from the zenith tropospheric delay, surface pressure is required to calculate the hydrostatic delay [Bevis *et al.*, 1992]. In this study, since surface pressure measurements were collected only at up to 7 GPS stations (Figure 1), surface pressures over other GPS stations were interpolated from the collected GPS meteorological data using the multireference differential model developed by Li [2004].

3. GPS/MODIS Integrated Model and Zenith Path Delay Difference Maps (ZPDDM)

[12] As MODIS-PWV is sensitive to the presence of clouds in the field of view, only MODIS-PWV values collected under clear-sky conditions can be used to correct

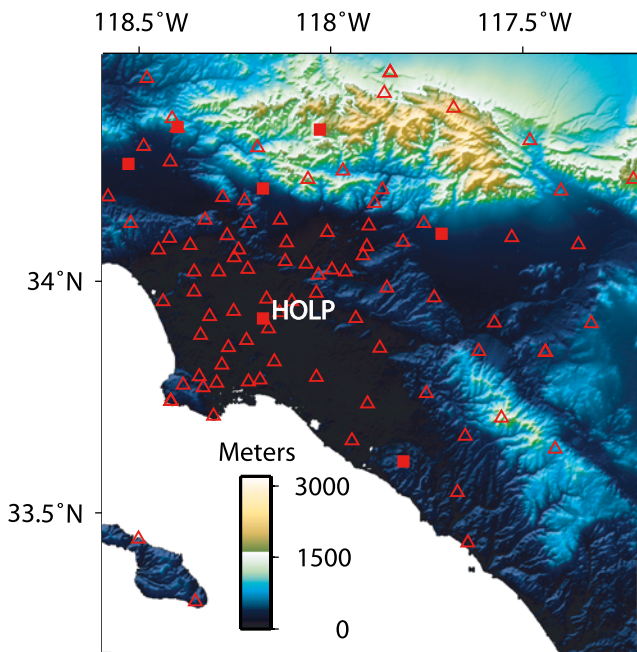


Figure 1. GPS stations available on 2 September 2000 superimposed on a 1-arc sec DEM from the Shuttle Radar Topography Mission (SRTM) [Farr and Kobrick, 2000]. Red solid squares represent GPS stations with meteorological data, and red open triangles represent GPS stations without meteorological data.

InSAR measurements. Therefore there are often missing values in MODIS near-IR water vapor fields due to clouds, which limit its applications. To identify cloud-free pixels, the cloud mask product used in this study had to indicate at least 95% confidence clear.

[13] In order to reduce the scale error of MODIS-PWV and fill in the missing values, a GPS and MODIS integrated approach developed by Li [2004] was used to provide regional high spatial resolution (resampled to around $200\text{ m} \times 200\text{ m}$) water vapor fields. First, MODIS-PWV values under cloud free conditions were selected using the cloud mask product. Second, a linear correction model was derived from a comparison between MODIS-PWV and GPS-PWV values under cloud free conditions. Third, the GPS-derived correction model was applied to calibrate the MODIS PWV values. Fourth, an improved inverse distance weighted interpolation method (IDW) was applied to fill in the cloudy pixels using only the corrected MODIS-PWV values and finally, the interpolated MODIS-PWV values under cloudy conditions were compared with the equivalent GPS-PWV estimates to validate the interpolated water vapor values. Applying this integration approach, the MODIS-PWV and GPS-PWV values agreed to within 1.6 mm (about 10 mm in ZWD) in terms of standard deviations, and the coverage of water vapor fields increased by up to 21.6% of the whole scene.

[14] The densified (or interpolated) MODIS 2-D water vapor fields can be used to derive zenith path delay difference maps (ZPDDM). In order to suppress the inherent noise of MODIS-PWV, a low-pass filter was

applied to the ZPDDM with an average width of around 2 km. Assuming pixel by pixel water vapor errors were uncorrelated, the accuracy of the ZPDDM increased by a factor of 2 at the expense of the spatial resolution (degraded to 2 km).

[15] Figures 2a and 2b show MODIS precipitable water vapor fields over Southern California collected on 2 September 2000 and 16 December 2000, respectively, that were used to generate ZPDDM (Figure 2c). Figure 2d shows the difference of zenith path delays after filling in the missing pixels using the GPS and MODIS integration method and applying a low-pass filter. Taking into account the standard deviation of the mean difference between GPS and corrected MODIS water vapor fields (1.6 mm), the conversion factor (around 6.2) to convert precipitable water vapor to zenith wet delays, and the smoothness by a low-pass filter with a $2\text{ km} \times 2\text{ km}$ window, it can be concluded that the uncertainty in ZPDDM is around 5 mm ($(1.6/\sqrt{2}) \times 6.2 \times \frac{1}{2} \times \sqrt{2} = 5\text{ mm}$). Note the GPS-corrected MODIS water vapor fields are assumed to have the same accuracy as GPS-derived precipitable water vapor values.

[16] It should be noted that this integration approach was developed and tested on the basis of a spatiotemporal correlation analysis using a dense GPS network (namely, Southern California Integrated GPS Network (SCIGN)) [Li, 2004]. The possibility to extend this approach to other situations where only one continuous GPS station is available is examined here. Figure 3a shows a spatial-temporal comparison between MODIS and GPS PWV over the SCIGN region, from which a linear correction model can be derived to calibrate MODIS PWV values as follows [Li, 2004]:

$$\text{MODIS-PWV(calibrated)} = 0.95 \times (\text{MODIS-PWV}) + 0.67 \quad (3)$$

Figure 3b shows a temporal comparison between MODIS and GPS PWV over the HOLP GPS station (Figure 1) during the period from 1 September 2000 to 31 August 2003, from which a linear correction model can be given as

$$\text{MODIS-PWV(calibrated)} = 0.94 \times (\text{MODIS-PWV}) + 0.75 \quad (4)$$

Since the phase of an interferogram is the difference of phase measurements between two different SLC images, what matters to the resultant corrected interferogram is the scale factors, rather than the zero-point offsets in equations (3) and (4). Taking into account the typical range of water vapor variation from 0 mm to 40 mm at midlatitudes, the difference between the calibrated MODIS-PWV values is only up to 0.4 mm when using equations (3) and (4), respectively, and can be neglected. This indicates that the GPS/MODIS integrated approach can also be applied when only one continuous GPS station is available in the MODIS coverage. This goal should be able to be met in most areas in the world taking into account the global distribution of the International GPS Service (IGS) stations and the wide coverage of MODIS near-IR water vapor products (i.e., $2,030\text{ km} \times 1,354\text{ km}$). For instance, the HARV IGS station is located at 34.47°N , 120.68°W within the same MODIS coverage as the area of interest in this study. It should be noted that a temporal correlation analysis has to be used in

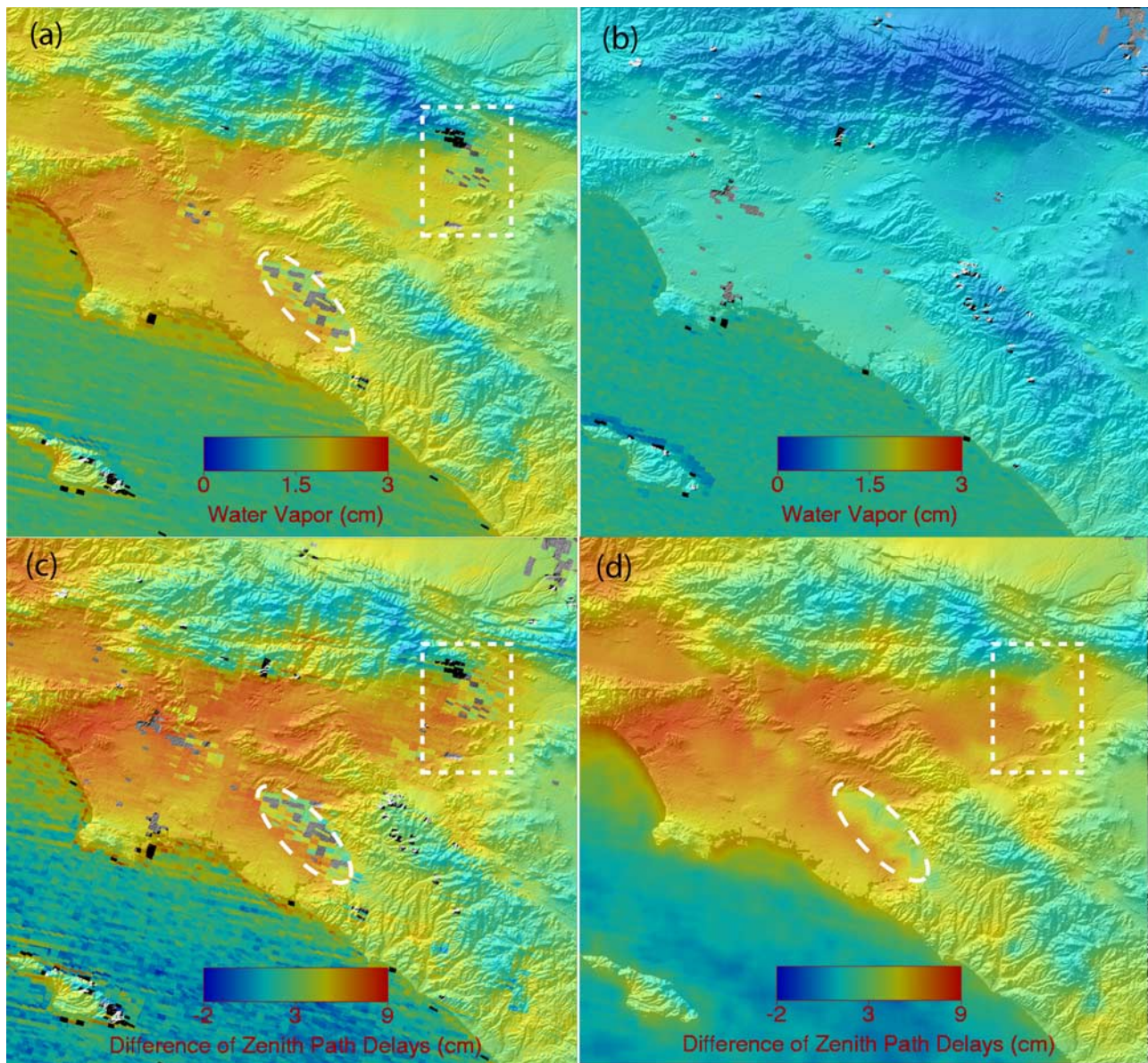


Figure 2. MODIS near-IR water vapor fields superimposed on a hill-shaded SRTM DEM. Both gray and black imply missing values due to the presence of clouds: (a) water vapor field collected on 2 September 2000; (b) water vapor field collected on 16 December 2000; (c) difference of zenith path delays; (d) difference of zenith path delays after filling the missing values and applying the low-pass filter. Both the dashed rectangle and oval represent the presence of clouds on 2 September 2000.

this case instead of the spatiotemporal correlation analysis used in the rest of this study.

4. Test Area and Processing Strategy

[17] The Southern California Integrated GPS Network (SCIGN, <http://www.scign.org>) is one of the densest regional GPS networks in the world with stations distributed throughout southern California. It is particularly dense in the greater Los Angeles metropolitan region. The SCIGN interstation spacing varies from only a few kilometers to tens of kilometers. The frequency of cloud free conditions is also high in southern California (see section 6). Therefore the Los Angeles region was selected as the principal test area.

[18] The surface of the Los Angeles region is deformed by both tectonic and nontectonic processes. The most rapid movements are nontectonic deformation due to groundwater and petroleum fluid level changes as shown by InSAR [e.g., *Bawden et al.*, 2001; *Watson et al.*, 2002]. *Bawden et al.* [2001] reported that parts of the Los Angeles basin exhibit seasonal vertical movement of up to 110 mm every year with a large portion of Santa Ana city sinking at a rate of 12 mm/yr over the period from 1997 to 1999. The seasonal rise and fall of several areas was attributed to annual variations in the elevation of the water table, confirmed by *Watson et al.* [2002] through their analysis of a longer span of data collected by ERS-1 and ERS-2 satellites between June 1992 and June 2000. Therefore, in order to validate the GPS/MODIS integrated water vapor correction

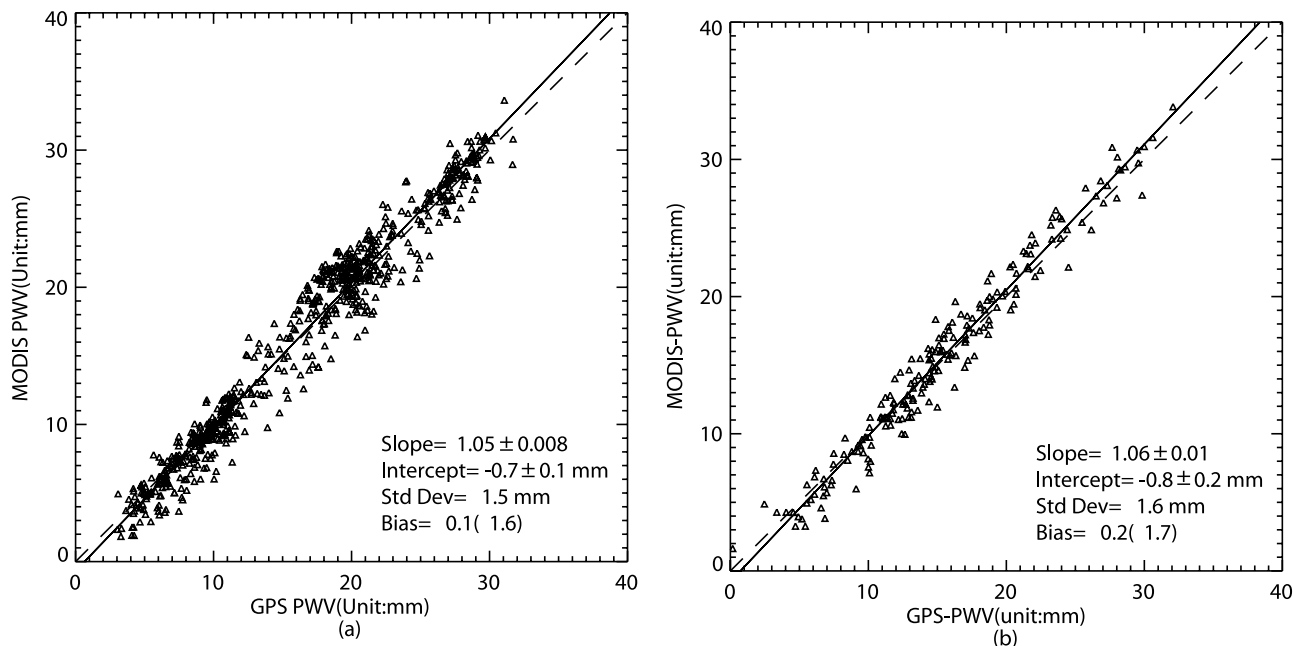


Figure 3. (a) Spatiotemporal comparison between MODIS and GPS PWV under cloud-free conditions over the SCIGN area [see Li, 2004]. The line of perfect fit (dashed line) and a least squares regression line (solid line) are plotted. The number of valid samples was 715, and 37 were omitted because of 2σ exclusion. (b) Temporal comparison between MODIS and GPS PWV under cloud-free conditions over the HOLP GPS station during the period from 1 September 2000 to 31 August 2003. The number of valid samples was 198, and 13 were omitted because of 2σ exclusion.

model using ERS-2 repeat-pass data, comparisons of deformation derived from InSAR and GPS techniques were performed through the mapping of GPS-derived displacements into the radar line of sight (LOS). Since seasonal horizontal movements of up to 14 mm were detected using GPS data [Bawden et al., 2001], GPS horizontal displacements must be included in the comparisons.

[19] In order to derive the 3-D displacements over each GPS station, precise coordinates were obtained from the “Modeled Coordinates by E-Mail Utility” provided by the Scripps Orbit and Permanent Array Center (SOPAC) (available at <http://sopac.ucsd.edu/cgi-bin/requestRefined-Coords.cgi>). These coordinates were based on a refined model including a linear trend, annual and semiannual fluctuations, offsets (coseismic or otherwise), and postseismic exponential decays and rate changes. All SOPAC parameters are estimated with full white noise + flicker noise covariances on the basis of a noise analysis of a time series of GPS positions. The a posteriori root-mean-square (RMS) noise is claimed to be nearly 1 mm (horizontally) and 3.5 mm (vertically) [Nikolaidis, 2002].

[20] The ERS-2 data used in this study (Table 1) were processed using the JPL/California Institute of Technology

ROI_PAC software [Rosen et al., 2004] as described below. This processing involved the usual steps of image coregistration, interferogram formation, baseline estimation from the precise orbits, and interferogram flattening and removal of the topographic signal by use of a 1-arc sec (~ 30 m) DEM from the Shuttle Radar Topography Mission (SRTM) [Farr and Kobrick, 2000] (Figure 1). At this point, the processing diverges from the usual interferometric processing sequence with the insertion of ZPDDM, which aims to reduce water vapor variations in the resultant interferograms. The ZPDDM is mapped from the geographic coordinate system to the radar coordinate system (range and azimuth) and subtracted from the interferogram. This corrected interferogram can be unwrapped and then used in baseline refinement. The wrapped, water-vapor-corrected interferogram is produced by subtracting the differential water vapor field from an original interferogram that has been flattened using the refined baseline and the precise DEM. In order to obtain the unwrapped water-vapor-corrected interferogram a new simulated interferogram, created using the refined baseline and topography, is subtracted from the unwrapped phase (including orbital ramp) with the water vapor model removed.

Table 1. Details of Interferograms Used in This Study

	Track	Frame	Date 1	Time Difference 1, ^a min	Date 2	Time Difference 2, ^a min	Δt , days	B_{\perp} , ^b m	σ , ^c rad
Ifm 1	170	2925	20 May 2000	+60	2 Sept. 2000	+50	105	13 to 37	0.18
Ifm 2	170	2925	2 Sept. 2000	+50	16 Dec. 2000	+45	105	-45 to -56	0.27
Ifm 3	170	2925	2 Sept. 2000	+50	23 Aug. 2003	+5	1085	88 to 89	0.43

^aTime difference between ERS and MODIS acquisitions. Positive implies that MODIS over pass time was later than ERS-2.

^bPerpendicular baseline at center of swath which varies along the track between the values shown.

^cPhase error due to the topographic uncertainty of SRTM DEM (7 m [Farr and Kobrick, 2000]).

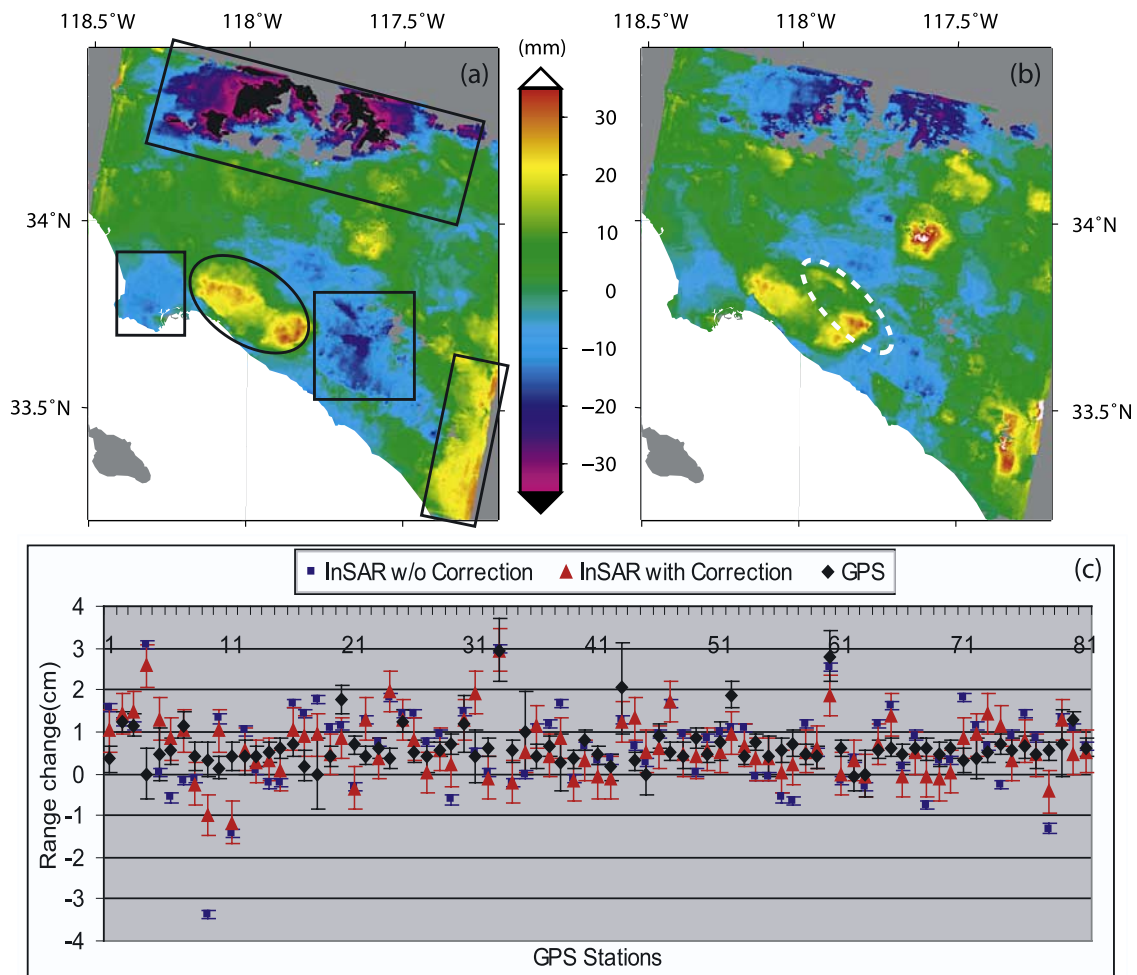


Figure 4. (a) Original Ifm: 000520–000902. Red means positive range change (ground moving away from satellite, see text). The black rectangles represent areas affected by water vapor, while the black oval indicates the Long Beach–Santa Ana basin exhibiting a subsidence. (b) Corrected Ifm using GPS/MODIS integrated water vapor fields. The white dashed oval indicates an uncertainty due to the presence of clouds. (c) Comparison of range changes derived from GPS and InSAR techniques in satellite line of sight (LOS). Note that positive range change means subsidence in the satellite LOS. The error bars imply (1) phase standard deviations of InSAR measurements (fixed to 1 mm, see text), (2) combined error from phase standard deviation and MODIS water vapor correction, and (3) the formal errors of GPS solutions. See discussions in section 4. Note that positive implies that the surface moves away from the satellite (i.e., the pixel exhibits subsidence), and negative implies uplift in LOS.

[21] As shown in Table 1, all pairs have small baselines, and the error in the SRTM DEM might lead to a phase error of up to 0.43 rad, which is well below the typical phase noise level of the ERS InSAR pairs, on the order of 40° (~ 0.70 rad) [Hanssen, 2001]. Therefore the topographic contribution can be considered negligible. Before comparisons, any residual orbital tilts and offsets remaining in interferograms were removed by subtracting a plane fitted to the unwrapped phase. In this paper, it should be noted that (1) the zero phase origin is in the center pixel of the interferograms; (2) the unwrapped phase has been converted to range change in millimeters and positive range change means ground moving away from satellite (if there is no atmospheric effect and any other error); and (3) the unwrapped phase has been shifted with a mean difference of range changes derived from GPS and InSAR when

compared to GPS-derived satellite line-of-sight (LOS) range changes.

5. Application Over SCIGN

[22] Figure 4 shows interferograms spanning the summer from 20 May 2000 to 2 September 2000. It is clear that water vapor effects over several areas (indicated by black rectangles) were significantly reduced after applying the GPS/MODIS integrated water vapor correction technique (Figure 4a versus 4b). In both Figures 4a and 4b, the Long Beach–Santa Ana basin (indicated by a black oval) showed up to 35 mm of subsidence in the summer of 2000. This result appears consistent with subsidence in the summer of 1999 measured by Bawden *et al.* [2001] and the annual cycle measured by Watson *et al.* [2002]. The smaller amplitude

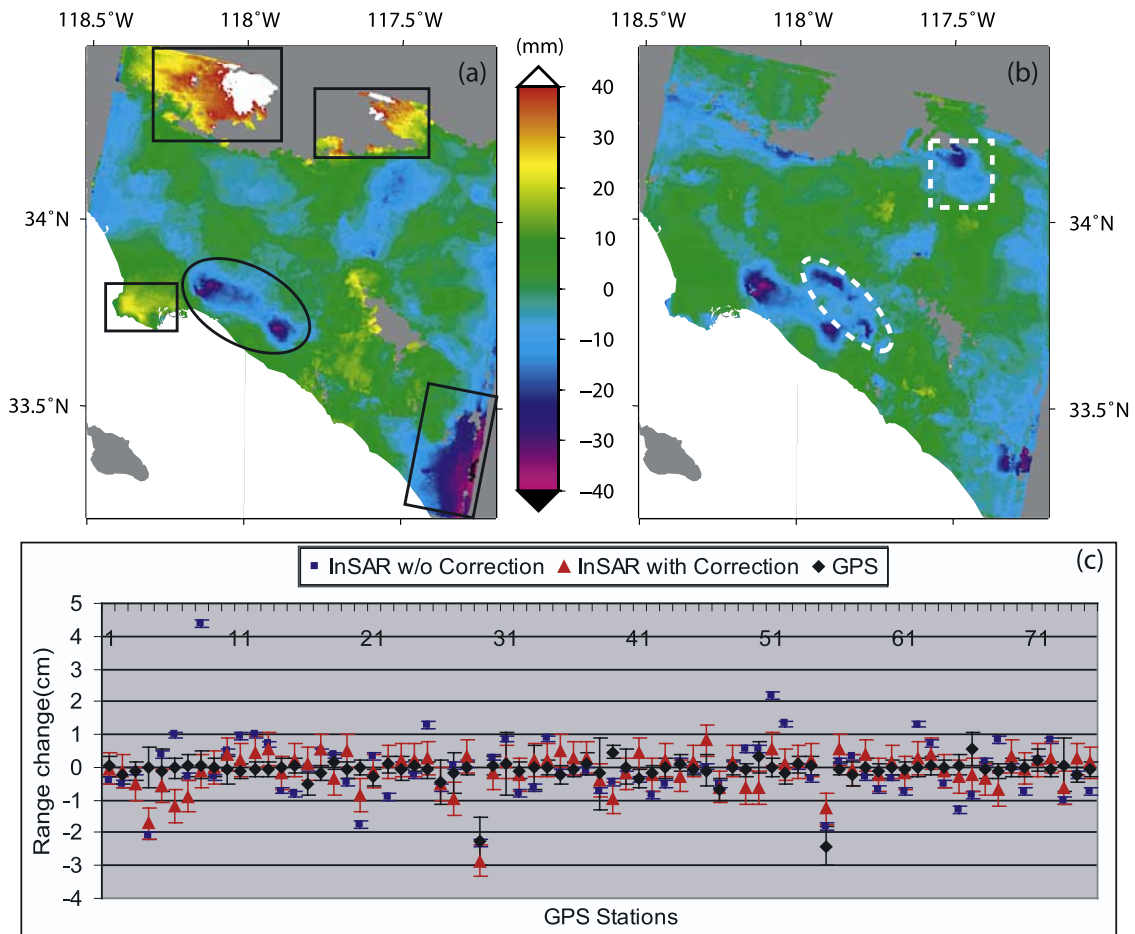


Figure 5. (a) Original Ifm: 000902–001216. The black rectangles represent areas affected by water vapor, while the black oval indicates the Long Beach-Santa Ana basin exhibiting an uplift. (b) Corrected Ifm using GPS/MODIS integrated water vapor fields. Both the dashed rectangle and oval represent uncertainties due to the presence of clouds on 2 September 2000. (c) Comparison of range changes derived from GPS and InSAR techniques in the satellite LOS. Note that positive range change means subsidence in the satellite LOS.

measured here (*Bawden et al.* [2001] reported maximum subsidence up to 60 mm) is partly due to the shorter time interval for interferogram (Ifm) 1. Phase variation of the unwrapped interferogram decreased from 2.66 rad without correction to 1.98 rad after applying the GPS/MODIS integrated water vapor correction model, implying that the unwrapped phase was much flatter after correction. Comparisons between GPS and InSAR range changes in the satellite LOS showed that the RMS difference decreased from 1.0 cm before correction to 0.7 cm after correction (Figure 4c), indicating that the GPS/MODIS integrated correction model improved the interferogram significantly.

[23] In Figure 4c, the error bars of each technique are shown. In this study, phase standard deviations were calculated by a weighted summation over a 5×5 pixel window after removing a local phase gradient from the wrapped differential interferograms after smoothing. The phase standard deviations were determined for both interferograms before water vapor correction and those after water vapor correction. It was observed that the phase standard deviations for both types of interferograms varied from 0.2 mm to 1.3 mm, which was far smaller than the typical phase noise

level of ERS InSAR pairs that is of the order of 40° (~ 3.1 mm) reported by *Hanssen* [2001]. This can be expected since a complex multilook of 8 (in range) \times 40 (in azimuth) was applied to the full-resolution interferogram followed by a power spectrum filtering ($\alpha = 0.6$, window size 32×32) [*Goldstein and Werner*, 1998] to reduce the phase noise in the interferograms. The correlation in the urbanized area of Los Angeles is also quite high so there is little noise coming from low correlation. It should be noted that there are numerous error sources that affect the accuracy of the phase values and may introduce systematic errors (biases) in the estimated topography and deformation fields that are not reflected in the phase standard deviation over small areas. They include satellite orbit errors, atmospheric disturbances, and residual topographic signals in differential interferograms [*Bürgmann et al.*, 2000]. Because the InSAR pairs had short baselines and a residual tilt was removed, the largest contribution to the remaining errors was atmospheric water vapor. In this paper, the error bars of InSAR results before correction were set to 1 mm since the phase standard deviations were around 1 mm and well below the typical phase noise level of the ERS InSAR pairs, while those after

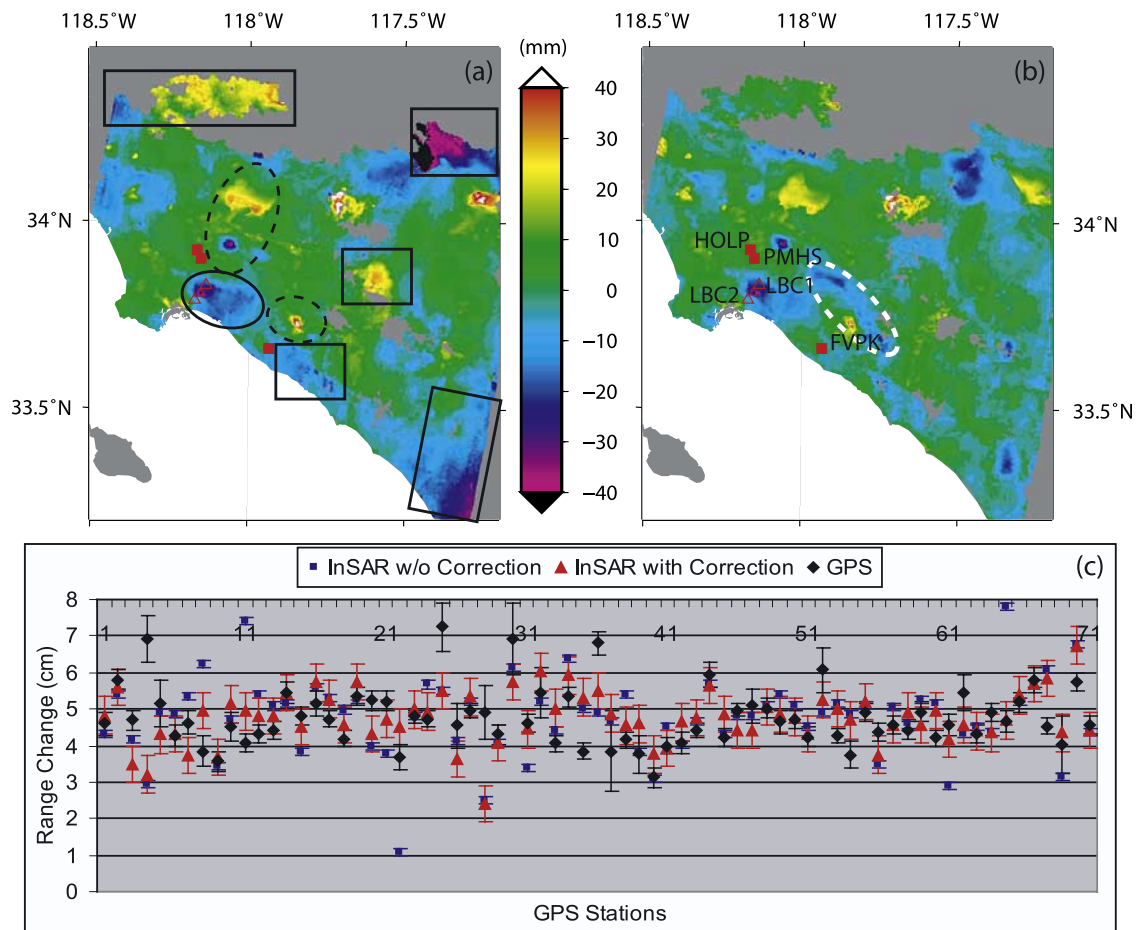


Figure 6. (a) Original Ifm: 000902–030823. The black rectangles represent areas affected by water vapor, while both the black solid and dashed ovals indicate surface deformation signals. (b) Corrected Ifm using GPS/MODIS integrated water vapor fields. The white dashed oval indicates an uncertainty due to the presence of clouds. (c) Comparison of range changes derived from GPS and InSAR techniques in the satellite LOS. Note that positive range change means subsidence in the satellite LOS.

correction were set to the quadratic sum of the phase standard deviation (namely, 1 mm) and the uncertainty of ZPDDM (namely, 5 mm).

[24] Ifm 2 spanning the autumn from 2 September to 16 December 2000 is shown in Figure 5. Like Ifm 1 (Figure 4), water vapor effects (indicated by black rectangles) were reduced significantly after applying our GPS/MODIS integrated water vapor correction model (Figures 5a and 5b). Phase variation of the unwrapped interferogram decreased from 2.48 rad before correction to 1.47 rad after correction, and the RMS difference between GPS and InSAR decreased from 1.1 cm before correction to 0.5 cm after correction (Figure 5c). Both Figures 5a and 5b show around 35 mm of uplift in the Long Beach-Santa Ana basin (indicated by a black oval) in the autumn of 2000, which is similar to the 34 mm of uplift in the late autumn in 1997 of *Bawden et al.* [2001].

[25] A long-term differential interferogram is shown in Figure 6, spanning the time interval between 2 September 2000 and 23 August 2003 (almost exactly 3 years). By comparing Figures 6a and 6b, we can easily discriminate surface deformation signals (indicated by black solid and dashed ovals) from water vapor effects (indicated by black

rectangles). From Figures 6a and 6b, an uplift of up to ~ 40 mm can be observed in the Long Beach-Santa Ana basin (indicated by the black solid oval). In order to validate the observed uplift, comparisons of relative range changes between different GPS stations in the satellite LOS were performed (Table 2). Both the LBC1 and LBC2 GPS stations are located within the observed uplift area indicated by the black solid oval, while the reference stations, i.e., FVPK, HOLP, and PMHS, are located on the margin of the Long Beach-Santa Ana basin, but outside the uplift area (see locations on Figures 6a and 6b). It is clear that in Table 2, all the relative range changes have the same positive sign except for the InSAR result without water vapor correction over the LBC2 station relative to the FVPK station. After water vapor correction, the sign also becomes positive. This indicates that both InSAR and GPS techniques can observe the uplift signals. *Bawden et al.* [2001] reported that a 2-year interferogram between October 1997 and October 1999 showed a subsidence of about 25 mm within the basin. Despite the fact that the 2 September 2000 and 23 August 2003 SAR images are very close to the same season, the variations in rainfall in different years might change the phase and amplitude of the seasonal aquifer

Table 2. Comparisons of Relative Range Changes in the Satellite LOS for Interferometer 3 (2 September to 23 August 2003)^a

Reference Station ^b	Relative Range Changes Over LBC1, cm			Relative Range Changes Over LBC2, cm		
	GPS ^c	InSAR Without Correction	InSAR With Correction	GPS ^c	InSAR Without Correction	InSAR With Correction
FVPK	0.3	1.5	1.9	1.2	-0.1	0.3
HOLP	1.9	3.0	3.1	2.8	1.4	1.4
PMHS	1.0	3.2	3.2	1.9	1.6	1.6

^aNote that positive relative range change means an uplift relative to the reference station in the satellite LOS.

^bReference stations are located outside the “uplift” area, but the LBC1 and LBC2 stations within the “uplift” area (Figure 6a).

^cThe range changes were derived from GPS heights only.

signal, so that our interferogram shows a net uplift over the 3-year time interval. Phase variation of the unwrapped interferogram decreased from 2.40 rad before correction to 1.60 rad after correction, and the RMS difference between GPS and InSAR decreased from 1.2 to 0.8 cm (Figure 6c). It should be noted that the positive range change (about 45 mm) of all the GPS stations in Figure 6c was primarily contributed by the horizontal components (i.e., east and north components), as Los Angeles is basically connected to the Pacific plate that is moving NW relative to the Earth, away from the descending ERS LOS. The range change derived from GPS heights only (used in Table 2) varied from -1.5 cm to 2.6 cm with an average of 0.04 cm.

[26] In Figures 4b, 5b, and 6b, an additional signal can be observed after correction (indicated by a white dashed oval). Using pair-wise logic [Massonnet and Feigl, 1995], the conclusion can be drawn that the feature must be generated in the MODIS water vapor field collected on 2 September 2000 since it was applied to all the three interferograms. On closer inspection of the MODIS water vapor fields, it was found that these signals were coincident with the presence of clouds on 2 September 2000 (Figure 2a), providing strong supporting evidence for the conclusion and suggesting that the spatial distribution and size of clouds may represent a limitation in the application of MODIS water vapor fields for InSAR atmospheric correction. Note that these signals are located at the edge of the Long Beach-Santa Ana basin close to the Santa Ana Mountains, where the water vapor field collected on 2 September 2000 exhibited a large gradient. This implies that the improved IDW method [Li, 2004] may have limited applicability to water vapor fields with large spatial variations, which is commonly the case in mountain areas. Similarly, the fringes indicated by a dashed rectangle are more likely due to the clouds on 2 September 2000 (Figure 5b versus Figure 2a). Caution therefore needs to be exercised when interpreting the results of the GPS/MODIS integrated water vapor correction model.

6. Conclusions and Future Work

[27] GPS and MODIS have been successfully integrated with InSAR measurements in this study. Their application to ERS-2 data over the SCIGN area indicates that even with time differences of up to one hour (shown in Table 1) between a MODIS and ERS-2 overpass, this GPS/MODIS integrated water vapor correction model not only helps discriminate geophysical signals from water vapor effects, but also reduces water vapor effects on interferograms significantly. Seasonal deformation was observed in the

Long Beach-Santa Ana basin, which is consistent with Bawden *et al.* [2001] and Watson *et al.* [2002].

[28] It has been shown that clouds affected the efficiency of the GPS/MODIS integrated correction approach. Therefore the frequency of cloud-free conditions over the SCIGN region was evaluated using a daily 1 km cloud mask product [Ackerman *et al.*, 1998]. In this paper, the frequency of cloud-free conditions refers to the probability of cloud-free occurrence. Figure 7 shows seasonal frequencies of cloud-free conditions during the period from 01 September 2000 to 31 August 2003: both the highest individual and average frequencies were found in summer (74% and 58%, respectively), while the lowest ones occurred in winter (2% and 36%). It is also clear that the frequencies varied from place to place in Figures 7a–7d. For example, the frequency over land was higher than that over the sea in summer, and the

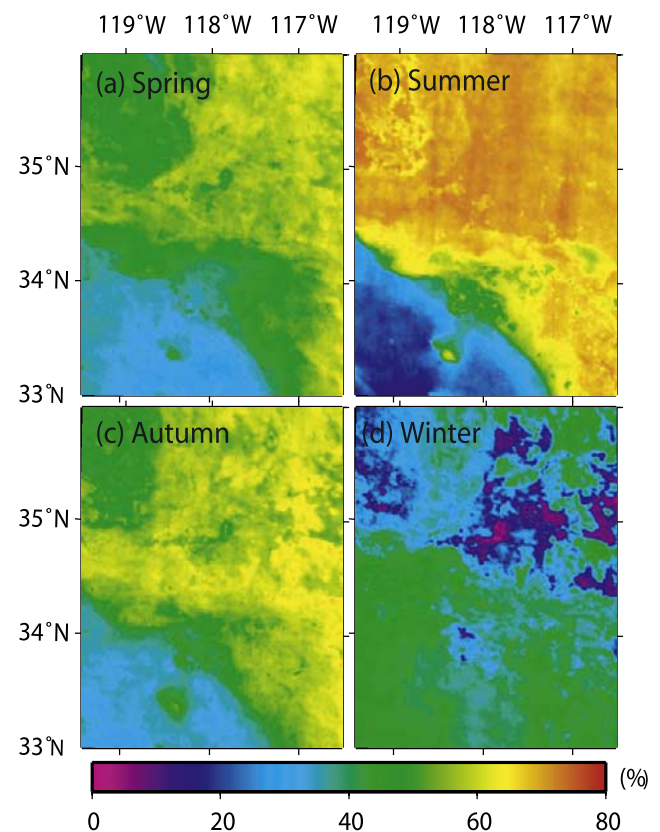


Figure 7. Seasonal frequencies of cloud-free conditions over the SCIGN region during the period from September 2000 to August 2003. Summer spans the months of June–August, and winter the months of December–February.

frequency over the Long Beach-Santa Ana basin was lower than that over other areas (Figure 7b). The average frequency of cloud free conditions was found to be 48%, with a maximum of 62% in the area during the whole 3 years. Since the revisit time of ERS-2 is 35 days, the statistical number of cloud-free ERS-2 SAR images, which can be obtained in 1 year, is 5. In reality, there were 16 scenes of cloud-free ERS-2 SAR images found in this study over the test area during the period from March 2000 to March 2003. Bearing in mind that the frequency of the cloud-free conditions is ~25% globally [Wylie and Menzel, 1999], a lack of cloud-free observations may be a major limitation to the application of the GPS/MODIS integrated correction model.

[29] In this paper, an improved IDW method [Li, 2004] was applied to fill in the missing values due to the presence clouds. Taking into account the height effects on water vapor variation which has been recognized by several previous researchers [e.g., Tarayre and Massonnet, 1996; Hanssen, 2001], an elevation-dependent turbulence model (Z. Li et al., Interferometric synthetic aperture radar atmospheric correction: GPS Topography-dependent Turbulence Model (GTTM), submitted to *Journal of Geophysical Research*, 2005) is expected to improve the interpolation in mountain areas. The next phase of this work would therefore be to combine the GPS/MODIS integrated correction model demonstrated in this paper with the turbulence model to estimate seasonal deformation and long-term subsidence rate in the Long Beach-Santa Ana basin.

[30] Finally, a typical wind speed of 8 m/s in California [Treuhaft and Lanyi, 1987] may advect "frozen" water vapor features by up to 28.8 km in one hour, indicating the time difference between MODIS and ERS-2 may be another limitation to the application of the GPS/MODIS integrated approach. It should be noted that the Medium Resolution Imaging Spectrometer (MERIS) onboard the ESA ENVISAT spacecraft can collect observations simultaneously with the Advanced Synthetic Aperture Radar (ASAR) during the daytime, and the MERIS water vapor product agreed with GPS-derived values to about 1.1 mm in terms of standard deviations (Z. Li et al., Assessment of the potential of MERIS near-infrared water vapour products to correct ASAR interferometric measurements, submitted to *International Journal of Remote Sensing*, 2004). Therefore the MERIS correction model is much more advantageous to ASAR than the GPS/MODIS integrated model is to ERS-2, and the integration of GPS, MERIS and InSAR is a particularly exciting possibility.

[31] **Acknowledgments.** This work is supported by an Overseas Research Students Award (ORS) and a UCL Graduate School Research Scholarship to Z. Li at University College London. This work is also associated with the NERC Earth Observation Centre of Excellence: Centre for the Observation and Modelling of Earthquakes and Tectonics (COMET). The work of E. Fielding was performed at the Jet Propulsion Laboratory, California Institute of Technology, under contract with NASA. We are grateful to T. J. Wright, M. Ziebart, and A. Sibthorpe for useful discussions and to H. Zebker, G. Wadge, and F. Sigmundsson for constructive reviews. We thank JPL/Caltech for the use of the ROI_PAC software to generate our interferograms [Rosen et al., 2004]. The ERS data were supplied under ESA ENVISAT data grant AO ID = 853 (HAZARDMAP), and the GPS data were obtained from the Scripps Orbit and Permanent Array Centre (SOPAC, http://sopac.ucsd.edu).

References

Ackerman, S. A., K. I. Strabala, V. B. Mendes, R. A. Frey, C. C. Moeller, and L. E. Gumley (1998), Discriminating clear sky from clouds with MODIS, *J. Geophys. Res.*, *103*(D24), 32,141–32,157.

- Bawden, G. W., W. Thatcher, R. S. Stein, K. W. Hudnut, and G. Peltzer (2001), Tectonic contraction across Los Angeles after removal of ground-water pumping effects, *Nature*, *412*(23), 812–815.
- Bevis, M., S. Businger, T. A. Herring, C. Rocken, R. A. Anthes, and R. H. Ware (1992), GPS meteorology: Remote sensing of atmospheric water vapor using the Global Positioning System, *J. Geophys. Res.*, *97*(D14), 15,787–15,801.
- Bock, Y., and C. A. Williams (1997), Integrated satellite interferometry in southern California, *Eos Trans. AGU*, *78*(29), 299–300.
- Bürgmann, R., P. A. Rosen, and E. J. Fielding (2000), Synthetic aperture radar interferometry to measure Earth's surface topography and its deformation, *Annu. Rev. Earth Planet. Sci.*, *28*, 169–209.
- Farr, T. G., and M. Kobrick (2000), Shuttle Radar Topography Mission produces a wealth of data, *Eos Trans. AGU*, *81*(48), 583, 585.
- Gao, B. C., and Y. J. Kaufman (2003), Water vapor retrievals using Moderate Resolution Imaging Spectroradiometer (MODIS) near-infrared channels, *J. Geophys. Res.*, *108*(D13), 4389, doi:10.1029/2002JD003023.
- Goldstein, R. M. (1995), Atmospheric limitations of repeat-track radar interferometry, *Geophys. Res. Lett.*, *22*(18), 2517–2520.
- Goldstein, R. M., and C. L. Werner (1998), Radar interferogram filtering for geophysical applications, *Geophys. Res. Lett.*, *25*(21), 4035–4038.
- Hanssen, R. F. (2001), *Radar Interferometry: Data Interpretation and Error Analysis*, 308 pp., Springer, New York.
- Li, Z. (2004), Production of regional 1 km × 1 km water vapor fields through the integration of GPS and MODIS data, paper presented at ION GNSS 2004, Inst. of Navig., Long Beach, Calif., 21–24 Sept.
- Li, Z., J.-P. Muller, and P. Cross (2003), Comparison of precipitable water vapor derived from radiosonde, GPS, and Moderate-Resolution Imaging Spectroradiometer measurements, *J. Geophys. Res.*, *108*(D20), 4651, doi:10.1029/2003JD003372.
- Massonnet, D., and K. L. Feigl (1995), Discrimination of geophysical phenomena in satellite radar interferograms, *Geophys. Res. Lett.*, *22*(12), 1537–1540.
- Massonnet, D., K. Feigl, M. Rossi, and F. Adragna (1994), Radar interferometric mapping of deformation in the year after the Landers earthquake, *Nature*, *369*, 227–230.
- Nikolaidis, R. (2002), Observation of geodetic and seismic deformation with the Global Positioning System, Ph.D. thesis, Univ. of Calif., San Diego.
- Nishihama, M., R. Wolfe, D. Solomon, F. Patt, J. Blanchette, A. Fleig, and E. Masuoka (1997), MODIS level 1A Earth location: Algorithm theoretical basis document (version 3.0), 147 pp., NASA Goddard Space Flight Cent., Greenbelt, Md.
- Rosen, P. A., S. Hensley, H. A. Zebker, and F. H. Webb (1996), Surface deformation and coherence measurements of Kilauea volcano, Hawaii, from SIR-C radar interferometry, *J. Geophys. Res.*, *101*(E10), 23,109–23,125.
- Rosen, P. A., S. Hensley, G. Peltzer, and M. Simons (2004), Updated repeat orbit interferometry package released, *Eos Trans. AGU*, *85*(5), 47.
- Tarayre, H., and D. Massonnet (1996), Atmospheric propagation heterogeneities revealed by ERS-1 interferometry, *Geophys. Res. Lett.*, *23*(9), 989–992.
- Treuhaft, R. N., and G. E. Lanyi (1987), The effect of the dynamic wet troposphere on radio interferometric measurements, *Radio Sci.*, *22*, 251–265.
- Watson, K. M., Y. Bock, and D. T. Sandwell (2002), Satellite interferometric observations of displacements associated with seasonal ground-water in the Los Angeles basin, *J. Geophys. Res.*, *107*(B4), 2074, doi:10.1029/2001JB000470.
- Williams, S., Y. Bock, and P. Fang (1998), Integrated satellite interferometry: Troposphere noise, GPS estimates, and implications for synthetic aperture radar products, *J. Geophys. Res.*, *103*(B11), 27,051–27,067.
- Wylie, D. P., and W. P. Menzel (1999), Eight years of high cloud statistics using HIRS, *J. Clim.*, *12*(1), 170–184.
- Zebker, H. A., P. A. Rosen, and S. Hensley (1997), Atmospheric effects in interferometric synthetic aperture radar surface deformation and topographic maps, *J. Geophys. Res.*, *102*(B4), 7547–7563.
- Zumberge, J. F., M. B. Hefflin, D. C. Jefferson, and M. M. Watkins (1997), Precise point positioning for the efficient and robust analysis of GPS data from large networks, *J. Geophys. Res.*, *102*(B3), 5005–5017.

P. Cross, Z. Li, and J.-P. Muller, Department of Geomatic Engineering, University College London, London, UK. (zhli@ge.ucl.ac.uk)
E. J. Fielding, Jet Propulsion Laboratory, California Institute of Technology, Pasadena, CA, USA.